Photoexcitation and predissociation intensities of the $c'\ ^1\Sigma_u^+$ ($v=3$ and 4), $c\ ^1\Pi_u$ ($v=3$ and 4), and $b'\ ^1\Sigma_u^+$ ($v=10$, 12, 13, and 15) states of N_2

C. W. Walter[a)]
Department of Physics and Astronomy, Denison University, Granville, Ohio 43023

P. C. Cosby
Molecular Physics Laboratory, SRI International, Menlo Park, California 94025

H. Helm
Fakultät für Physik, Albert-Ludwigs Universität, 79104 Freiburg, Germany

(Received 24 September 1999; accepted 16 December 1999)

Photofragment spectroscopy is applied to investigate perturbations in the photoexcitation and predissociation of excited singlet states of N_2. Discrete rovibrational levels in the Rydberg states $c'\ ^1\Sigma_u^+$ ($v=3$ and 4) and $c\ ^1\Pi_u$ ($v=3$ and 4) and in the valence state $b'\ ^1\Sigma_u^+$ ($v=10$, 12, 13, and 15) are prepared by laser excitation from the metastable $a''\ ^1\Sigma_g^+$ ($v=0$) state in a fast (3 keV) molecular beam. Fragment atoms produced by predissociation are monitored as a function of exciting laser frequency using a position- and time-sensitive detector to measure the photofragment intensity distribution in the rovibrational bands. The photofragment spectra show extreme departures from normal rovibronic intensity distributions due to strong perturbations in the two highly mixed complexes: $c'(3)/c(3)/b'(10)$ and $c'(4)/c(4)/b'(13)$. The measured photofragment intensities are compared to photoexcitation line strengths calculated using a comprehensive model of the Rydberg-valence state mixing [Stahel, Leoni, and Dressler, J. Chem. Phys. **79**, 2541 (1983)]. This theoretical model accurately predicts most of the variations in the photofragment intensities, and reveals the causes of the perturbations. For the states investigated in the present study, the primary factor that determines the photofragment intensity is the degree of b' character of the state, which favorably affects both photoexcitation and predissociation. Interference effects are found to be important in determining absorption intensities in N_2. © *2000 American Institute of Physics.* [S0021-9606(00)01410-0]

I. INTRODUCTION

The properties of molecular nitrogen are important for both fundamental and practical reasons. As the primary component of Earth's atmosphere, and that of the planetary moons Titan and Triton, N_2 participates in a variety of important atmospheric processes such as absorption of extreme ultraviolet solar radiation,[1] radiative energy transfer and atmospheric airglow,[2,3] and atmospheric chemistry.[1,4–6] The dominant source of atomic nitrogen in the quiet daytime thermosphere of Earth is predissociation of molecular nitrogen following photoexcitation or electron impact excitation of N_2.[1,7,8] Clearly, in order to accurately model planetary atmospheres, the excitation and decay properties of molecular nitrogen must be understood in detail.

The absorption spectrum of N_2 from the ground state $X\ ^1\Sigma_g^+$ includes many irregular bands belonging to several highly mixed Rydberg and valence states. The lowest dipole-allowed transitions reach singlet ungerade states in the energy range 100 800–120 000 cm^{-1} above the ground state, including the valence states $b'\ ^1\Sigma_u^+$ and $b\ ^1\Pi_u$ and the Rydberg states $c'\ ^1\Sigma_u^+$, $e'\ ^1\Sigma_u^+$, $c\ ^1\Pi_u$, $e\ ^1\Pi_u$, and $o\ ^1\Pi_u$. Potential energy curves[9] for the relevant states are shown in Fig. 1. The energy levels of these bands and their absorption and emission intensities show strong perturbations due to both homogeneous and heterogeneous interactions.[10–23] In addition to perturbations leading to level shifts, significant predissociation has been observed in many of these excited singlet states.[8,20–30]

Mixing between the singlet states of N_2 has been treated in detail in the comprehensive work of Stahel, Leoni, and Dressler.[31] Their theoretical model derives diabatic potential curves, electronic couplings, and transition moments from fitting experimental data for 71 vibrational levels of the singlet Rydberg and valence states. The model has been extended to include rotational effects[32] by Helm, Hazel, and Bjerre[27] and more recently by Edwards *et al.*[33] The diabatic state deperturbation model facilitates calculation of the rovibrational energies, fractional electronic characters, and absorption and emission oscillator strengths for the observed perturbed states.

To investigate photoexcitation and predissociation of singlet nitrogen in the present work, we have measured the relative photofragment intensity in laser scans of absorption bands from the metastable $a''\ ^1\Sigma_g^+$ ($v=0$) state to the states c' ($v=3$ and 4), c ($v=3$ and 4), and b' ($v=10$, 12, 13, and 15); results of similar studies for b' ($v=9$, 11, 14, 16, 17, and 18), o ($v=3$ and 4), e' ($v=0$), and e ($v=0$) will be reported in a second paper.[34] The atomic fragments produced

a)Electronic mail: walter@denison.edu

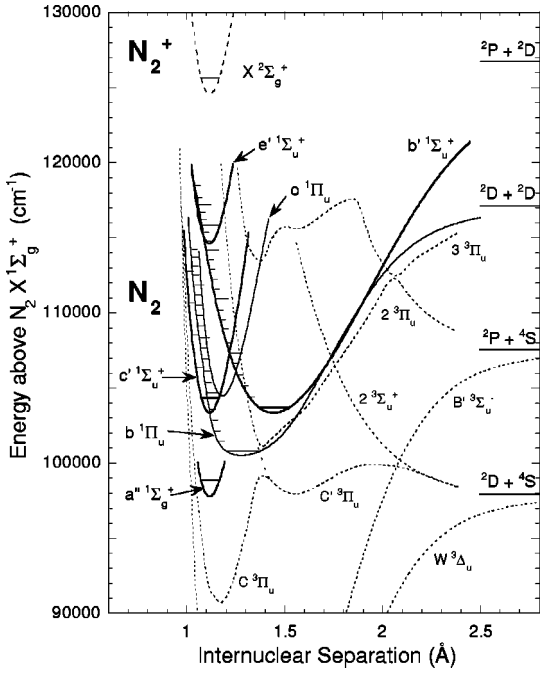

FIG. 1. Selected potential energy curves of N_2. The initial state, $a''\,^1\Sigma_g^+$, and the excited $^1\Sigma_u^+$ and $^1\Pi_u$ states studied in the present work are shown by the solid curves. Note that the potential energy curves of the $c\,^1\Pi_u$ and $e\,^1\Pi_u$ states are indistinguishable from those of $c'\,^1\Sigma_u^+$ and $e'\,^1\Sigma_u^+$, respectively, on the scale of this figure and are not shown. All possible triplet *ungerade* states, which can participate in predissociation of the singlets, are shown by dashed curves, as is the ground electronic state of N_2^+. The sources of the curves are given in Ref. 9, and Refs. 43–45.

by predissociation of laser excited states are monitored using a fast beam apparatus equipped with a position- and time-sensitive detector for product atom identification.[35] The observed photofragment intensity depends on the product of the transition line strength for excitation of the particular rovibrational level and the predissociation fraction η for that level. The measured photofragment intensities are compared to transition line strengths calculated using the diabatic state deperturbation model of Stahel, Leoni, and Dressler[31] with the inclusion of rotational coupling in the Rydberg mixing.[27]

Perturbations within rovibrational bands are identified and investigated by comparison of the measured photofragment intensities to the calculated transition line strengths. The strong mixing of Rydberg and valence states leads to dramatic changes in the electronic character of rotational levels within some vibrational states, resulting in shifts in level energies and substantial deviations from normal rovibronic intensity distributions. Interference effects also play an important role in determining excitation strengths. In most cases the perturbations are accurately predicted by the theoretical model, with very good agreement between the measured and calculated intensities for most bands studied here.

The states studied here form two highly mixed complexes: $c'(3)/c(3)/b'(10)$ and $c'(4)/c(4)/b'(13)$. For these states, the primary factor that determines excitation strength is identified to be the fractional diabatic b' character of the state; this is due to favorable vibrational overlap for photoexcitation of the diabatic b' state from the $a''(0)$ lower state in this energy range. All of the states studied are strongly predissociated, with branching fractions for predissociation of greater than 0.5.[29] The predissociation fractions for most of the vibrational states show little rotational dependence; however, both the $c'(4)$ and $c'(3)$ states show moderate increases in the degree of predissociation with increasing rotational level, with the $c'(3)$ showing a slight decrease in predissociation above $J=14$. The rotational dependencies observed for $c'(3)$ and $c'(4)$ in the present study are consistent with the predissociation fractions determined recently by Ajello, James, and Ciocca using comparisons of excitation and emission cross sections for individual rotational levels.[23] The present results yield new insight into perturbations in singlet nitrogen and provide a striking demonstration of the predictive power of the diabatic state model developed by Stahel, Leoni, and Dressler.[31]

II. THEORETICAL MODEL

The theoretical model used in the present studies to describe the mixing of excited states in nitrogen is an extension of the model originally developed by Stahel, Leoni, and Dressler.[31] The details of the present procedure for calculation of the mixing have been reported previously,[27] therefore only a brief discussion is given here.

In their model, Stahel, Leoni, and Dressler treated a total of 71 interacting vibrational levels of the six lowest excited singlet electronic states of N_2: the valence states $b'\,^1\Sigma_u^+$ ($v\leqslant 28$) and $b\,^1\Pi_u$ ($v\leqslant 19$), and the Rydberg states $c'\,^1\Sigma_u^+$ ($v\leqslant 8$), $e'\,^1\Sigma_u^+$ ($v\leqslant 2$), $c\,^1\Pi_u$ ($v\leqslant 4$), and $o\,^1\Pi_u$ ($v\leqslant 4$). By fitting observed term energies, they derived deperturbed diabatic potential energy curves for the rotationless ($J=0$) states and electronic coupling matrix elements for the homogeneous interactions. Using these results, they then determined electronic transition moments from the ground state to these diabatic states by fitting calculated intensities to experimental electron energy loss intensities. Carroll and Hagim[32] applied this model to $^{15}N_2$ and to rotationally excited levels. Helm, Hazell, and Bjerre[27] extended the model to include the centrifugal contribution to the potential curves and the heterogeneous rotational coupling between the c' and c Rydberg states. A similar extension of the Stahel, Leoni, and Dressler model has also been reported by Edwards *et al.*[33]

The perturbed states are represented in the basis set of diabatic unperturbed states by diagonalization of the interaction matrix to obtain the eigenvalues (term energies) and eigenvectors (combinations of basis states). Each perturbed electronic state u of rovibrational level (v',J') is represented as a linear combination of diabatic basis states:

$$|u,v',J'\rangle=\Sigma_i C_i|i,v_i',J'\rangle, \tag{1}$$

where C_i, the coefficient of the ith basis state, is obtained from the matrix diagonalization. The fractional diabatic electronic state character of a perturbed level is given by the coefficient for that basis state squared:

$$P_i=|C_i|^2. \tag{2}$$

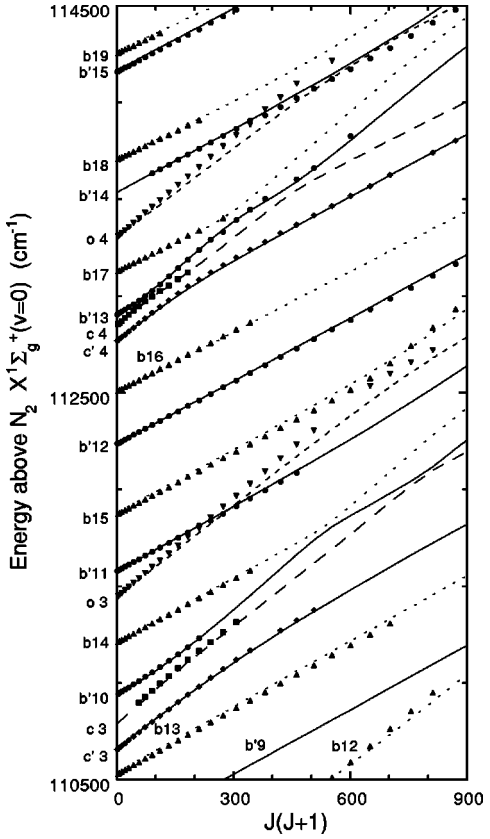

FIG. 2. Term energies for N_2 singlet states in the energy range from 110 500 to 114 500 cm^{-1} as a function of rotational level $J(J+1)$. Symbols give the observed energies of rovibrational levels; solid and dashed lines give the calculated energies from the diabatic state mixing model of the $^1\Sigma_u^+$ and $^1\Pi_u$ states, respectively. The observed energies are determined from the present work and from Refs. 12, 14, and 16.

The character is then summed for all vibrational levels of the individual diabatic electronic states to obtain the fractional character of b', b, c', e', c, and o for each perturbed rovibrational level.

A first assessment of the quality of the deperturbation model can be made by comparison of the calculated rovibrational term energies to the observed values, which is shown in Fig. 2 for the states studied in the present work. As the graph demonstrates, the calculated term energies (shown as lines) are in very good agreement with observation (shown as symbols) for most levels, even within the highly mixed $c'(3)/c(3)/b'(10)$ and $c'(4)/c(4)/b'(13)$ complexes. The term energies and state assignments are discussed further in the following.

The diabatic state mixing model facilitates calculation of the intensities for photoexcitation of the singlet states, which can then be compared to the measured photofragment intensities obtained in the present experiments. The line strength for a transition from a rovibrational level in a lower electronic state (l,v'',J'') to an upper level (u,v',J') is the square of the transition moment for the excitation:[36]

$$S_{u,v',J';l,v'',J''}=|\langle u,v',J'|\mu|l,v'',J''\rangle|^2, \tag{3}$$

where μ is the electric dipole matrix operator. In the present calculations, the upper state is replaced by its diabatic basis state expansion, given by Eq. (1), yielding

$$S_{u,v',J';l,v'',J''}=|\Sigma_i C_i\langle i,v_i',J'|\mu|l,v'',J''\rangle|^2. \tag{4}$$

In Eq. (4), it is important that the summation of transition moments be performed before squaring in order to account for interference in the contributions to the line strength from different basis states.

It is calculationally convenient, as well as instructive, to separate the line strength into electronic, vibrational, and rotational components. Equation (4) for the line strength can be recast as[36]

$$S_{u,v',J';l,v'',J''}=|\Sigma_i C_i\langle v_i'|v''\rangle R_e^i(\underline{S}_{J'J''})^{1/2}|^2, \tag{5}$$

where R_e^i is the electronic transition moment between the lower state and the ith upper diabatic basis state, $\langle v_i'|v''\rangle$ is the vibrational overlap integral, and $\underline{S}_{J'J''}$ is the Hönl–London rotational line strength factor for the particular branch and electronic symmetries of the transition.

In the present calculations, Eq. (5) is used to obtain the transition line strength for excitation of the singlet states from the lower state $a''\ ^1\Sigma_g^+\ (v=0)$, which is used as the initial state for photoexcitation in the experiments. The diabatic basis state coefficients for the perturbed states are calculated from the matrix diagonalization using the interaction matrix elements given in Stahel, Leoni, and Dressler[31] with the inclusion of rotational coupling between the c' and c Rydberg states.[27]

The vibrational overlap integrals between $a''(0)$ and the diabatic basis states are numerically calculated directly from the potential curves. The a'' potential energy curve used in the present work[37] is derived from the measurements of Hanisco and Kummel.[38] The calculated vibrational overlap integrals for transitions from $a''(0)$ are given in Table I. The magnitudes of the vibrational overlaps can be understood qualitatively from the potential energy curves shown in Fig. 1. The potential curves of the diabatic c', c, and e' Rydberg states, which are built on the core of the $N_2^+\ X\ ^2\Sigma_g^+$ ground state ion, are very similar in shape to the a'' state, leading to strong vertical overlap for (0,0) transitions but much weaker overlap for transitions from $a''(0)$ to excited vibrational levels of the Rydbergs. The diabatic o Rydberg state, which is built on the core of the excited $A\ ^2\Pi_u$ ion, extends to greater internuclear separations and therefore has good overlap with $a''(0)$ for several vibrational levels. In contrast to the Rydbergs, the potential curves of the diabatic b' and b valence states are much wider than that of a'' and their minima are at larger internuclear separation. The shapes and placements of the potential curves lead to good overlap with $a''(0)$ for the medium vibrational levels $(v'=6-21)$ of the diabatic b' state, while the diabatic b state has good overlap with $a''(0)$ over the narrower range of $v'=1-11$. The calculated vibrational overlaps with the $a''(0)$ state are similar to those obtained for overlaps with the ground state $X(0)$ by Stahel, Leoni, and Dressler; this is due to the very similar potential curves of the a'' and X states.

The electronic transition moments R_e derived by Stahel, Leoni, and Dressler for excitation from the ground state $X\ ^1\Sigma_g^+\ (v=0)$ are used without modification in the present calculations for excitation from the $a''(0)$ state; the values are given in Table II. This substitution is reasonable because

TABLE I. Vibrational overlap integrals between $a''(0)$ and the b' and b valence and c', c, e', and o Rydberg states of N_2.

v	b'	b	c'	c	e'	o
0	0.002	0.095	1.000	0.982	0.999	0.660
1	0.006	0.200	−0.028	−0.191	−0.042	0.546
2	0.014	0.300	−0.006	−0.011	−0.006	0.385
3	0.028	0.372	−0.011	−0.001		0.257
4	0.049	0.405	−0.004	0.000		0.170
5	0.078	0.400	−0.002			
6	0.113	0.366	−0.001			
7	0.153	0.316	0.000			
8	0.196	0.260	0.001			
9	0.237	0.206				
10	0.274	0.158				
11	0.304	0.119				
12	0.322	0.088				
13	0.329	0.064				
14	0.324	0.046				
15	0.309	0.033				
16	0.284	0.023				
17	0.253	0.016				
18	0.219	0.012				
19	0.183	0.008				
20	0.149					
21	0.118					
22	0.090					
23	0.067					
24	0.048					
25	0.034					
26	0.022					
27	0.014					
28	0.008					

of the identical electronic symmetries and very similar potential curves of the a'' and X states. In the present case, the calculated line strengths are fairly insensitive to the relative magnitudes of the electronic transition moments, because the vibrational overlaps are so much stronger for transitions to the diabatic b' levels than to the other diabatic singlet states in this energy range that the b' contribution to the transition moment completely dominates the line strength.

In cases of strong mixing between states that have appreciable transition moments, interference effects are critical in determining the line strengths, and the relative signs of the individual transition moments become important. The transition moment associated with each diabatic basis state, given by Eq. (5), contains three signed quantities: the basis state coefficient C_i, the vibrational overlap integral $\langle v_i'|v''\rangle$, and the electronic transition moment R_e^i. The phase of the vibrational overlap integral comes directly from the potential energy curves used in the calculation. The signs of the basis state coefficients and electronic transition moments are derived from the fitting of experimental term energy and intensity data carried out by Stahel, Leoni, and Dressler.[31] As discussed in the following, the good agreement in the present work between calculated and measured intensities for most rovibrational transitions in which interference is important demonstrates that the phases used for calculation of the line strength are fairly reliable.

TABLE II. Electronic transition moments from $a''(0)$ to the diabatic b', b, c', c, e', and o states. Values are taken as the transition moments from $X(0)$ derived by Ref. 31.

Diabatic state	R_e
b'	0.8243
b	0.6628
c'	−0.5946
c	−0.2261
e'	−0.2842
o	0.1161

The calculated line strengths for rovibrational transitions from $a''(0)$ to the perturbed states b' ($v'=10$, 12, 13, and 15), c' ($v'=3$ and 4), and c ($v'=3$ and 4) are shown in Figs. 5–11, together with the experimentally measured photofragment intensities. The results are discussed in the following.

III. EXPERIMENTAL METHOD

The photofragment spectrometer used in the present studies has been described in detail previously.[24,28] Briefly, in a high vacuum apparatus, N_2^+ ions are extracted from an ion source (both an electron-impact and a hollow-cathode discharge ion source were used in the present experiments), accelerated to 3 keV and formed into a beam, then mass selected with a sector magnet. The ion beam then passes through a 10-mm-long cesium charge transfer cell. Electron capture from cesium produces fast neutral nitrogen molecules, some of which are in the metastable $a''\ ^1\Sigma_g^+$ state at an energy of 12.3 eV above the ground state which is used as a precursor for photoexcitation of highly excited singlet states of N_2. The lifetime of the a'' ($v=0$) state is 3.5 μs.[39] This state is an excellent initial state for photoexcitation studies of nitrogen because its electronic configuration is the same as that of ground state N_2 ($X\ ^1\Sigma_g^+$) and because the similarity of their potential curves leads to very similar vibrational overlaps for photoabsorption to the excited singlet ungerade manifold.

Residual ions are deflected out of the beam after the charge transfer cell and the remaining neutral beam passes through a narrow slit 54 cm from the charge transfer cell. Immediately after the slit, the neutral beam is intersected by the intracavity beam of a tunable cw laser, in this case either a dye- or titanium:sapphire laser pumped by an argon ion laser. Undissociated molecules are collected by a narrow beam flag situated 10 cm downstream from the slit. Dissociation fragment atoms with sufficient transverse velocity to avoid the flag continue in the original beam direction until they impact a position- and time-sensitive detector, located 110.5 cm from the laser interaction region. The detector[35] measures the radial separation and arrival time difference between the correlated pair of fragment atoms produced by single molecular dissociation events from which the center-of-mass translational energy released in the dissociation, W, is obtained.

The photofragmentation scheme used in the present experiments is represented by the reaction

$$N_2(a''(v''=0,J''))+h\nu\rightarrow N_2^*(v',J')\rightarrow N+N+W$$

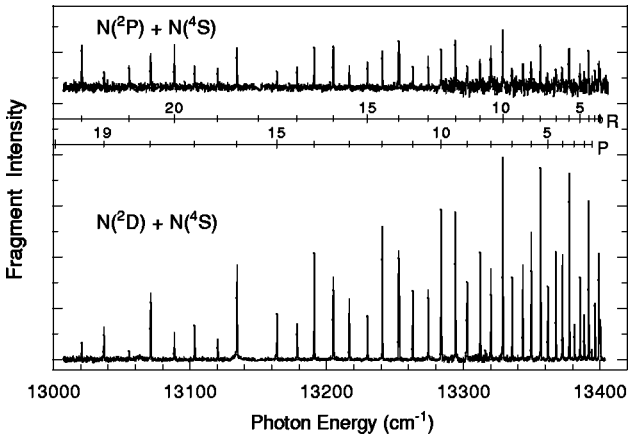

FIG. 3. Energy binned photofragment spectra as a function of photon energy showing the P and R branches of the $b'(12)\leftarrow a''(0)$ band normalized to neutral beam flux and intracavity laser power. The lower trace shows $N(^2D)+N(^4S)$ fragmentation; the upper trace shows $N(^2P)+N(^4S)$ fragmentation.

in which a selected rovibrational level of N_2 is prepared by absorption of a laser photon of frequency ν. The photoexcited molecule may subsequently predissociate, releasing an amount of translational energy W that is shared equally between the two equal mass atoms. Since the energy of the photoexcited level is known from the absorption spectrum, the electronic states of the product atoms can be inferred from the W release on the basis of energy conservation.

The photofragment intensity as a function of rovibrational level is measured by scanning the laser frequency while monitoring the photofragment signal, laser power, and neutral beam flux. Bound–bound transitions from N_2 a'' $(v''=0,J'')$ to specific predissociated excited rovibrational levels appear as sharp peaks in the photofragment energy release spectrum. The transition line widths for individual rotational lines of some of the states studied here are in the range 0.02–0.07 cm^{-1},[25,27] which is much narrower than the present laser linewidth of $\sim$0.5 cm^{-1}. Both the absorbing level $[a''(v''=0,J'')]$ and the dissociating level [e.g., $b'(v'=12,J')$] are identified from rotational analysis of the excitation spectrum with the aid of spectroscopic information in the literature.[31,12,14,19] At each laser frequency setting, the translational energy release W for each detected photofragment coincidence pair is measured, and this measurement is repeated for many molecules to acquire a statistically significant representation of the photofragment intensity. The coincidences at a particular frequency setting are then grouped into eight separate bins according to W, with each bin encompassing a different range of energy release. A three-dimensional excitation spectrum is thus obtained: photofragment signal versus laser frequency versus energy release.

An example of the energy binned photofragment spectra is shown in Fig. 3, which shows a laser frequency scan over the $b'(12)\leftarrow a''(0)$ band. This spectrum was obtained by accumulating the photofragment signal for 5 s at each frequency setting and stepping the laser in increments of $\sim$0.2 cm^{-1}. In Fig. 3, the coincidences in the bins corresponding to dissociation from $b'(12)$ rotational levels to the $N(^2D)+N(^4S)$ and $N(^2P)+N(^4S)$ limits are displayed separately. The product state branching between these two dissociation limits has been measured previously by our group for $b'(12)$ and several other rovibrational bands.[24,28] To obtain the relative photofragment intensity, the measured coincidence signal for each dissociation limit is divided by the calculated solid-angle collection efficiency of the detector for that particular energy release,[28] and the two signals are summed to give the total photofragment signal. The total signal is then scaled by the measured intracavity laser power and the neutral beam flux for normalization.

To obtain the relative photofragment intensity for individual transitions, each peak is fit by a Gaussian function of constant width and the intensity is taken as the amplitude of the fitted peak. The constant width used for determining the peak height is the average width of the peaks obtained when the width is allowed to vary in the fitting program. The constant peak width used in the present analysis is 0.54 cm^{-1}, which corresponds approximately to the linewidth of the laser. Fitting each peak is necessary to obtain the greatest consistency in comparisons from one peak to another, because each peak is traversed in only four to five steps of the laser frequency. Thus individual peaks may be somewhat asymmetric and the highest data point may not be at the maximum of the true line shape. The fitting procedure greatly reduces this random uncertainty. The P and R branches are independently analyzed yielding two separate measurements of the photofragment intensity for all upper state rotational levels in which the transitions are unblended.

IV. RESULTS AND DISCUSSION

The rotational dependence of excitation and predissociation within a band is determined by comparison of the observed photofragment intensities to the calculated photoexcitation line strengths. The photofragment intensity for a particular upper level J', $N_{pJ'}$, is proportional to the product of three factors: the relative initial population of the lower state rotational level $N_{J''}$, the line strength for photoexcitation from the lower level to the upper level $S_{u,v',J';l,v'',J''}$, and the fraction of upper state molecules that predissociate η:

$$N_{pJ'}\sim \eta S_{u,v',J';l,v'',J''}N_{J''}. \tag{6}$$

As discussed in Sec. II, the line strength $S_{u,v',J';l,v'',J''}$ can be further separated into the product of the electronic transition moment R_e, the vibrational overlap interval $\langle v'|v''\rangle$, and the Hönl–London rotational line strength factor $\underline{S}_{J'J''}$, as given by Eq. (5).

If both the lower and upper states are unperturbed, then the electronic and vibrational terms in the line strength should be nearly constant within a particular vibrational band and the rotational dependence is contained entirely in the standard Hönl–London factor.[40] However, if the upper state is perturbed by J-dependent interactions with other states, as is the case for most of the excited singlet states studied in the present work, both the electronic and vibrational terms can vary significantly with rotational level. This rotational variation appears as perturbations in the measured photofragment intensity within a rovibrational band. Comparison of the measured photofragment intensity to the calculated line

strength from the theoretical model of Rydberg-valence mixing characterizes the perturbations leading to changes in the intensity, tracks changes in the predissociation factor, and provides a stringent test of the diabatic state deperturbation model.

In order to obtain the desired information about excitation and predissociation, it is first necessary to determine the initial rotational distribution of the a'' $(v=0)$ lower state, $N_{J''}$, so that this population can be accurately accounted for in the comparison of the measured photofragment intensity to the calculated line strength.

A. Lower state a'' $(v=0)$ rotational distribution

The rotational distribution of the N_2^+ ions extracted from the ion source is expected to be a thermal Boltzmann distribution at an appropriate temperature for the source. The rotational distribution that exists in the ions prior to charge neutralization should be transferred almost directly to the excited N_2 a'' $(v=0)$ molecules formed by charge neutralization, because the long-range nature of the near-resonant charge transfer process results in a relatively gentle collision that closely preserves the rotational population of the molecule.[41]

The lower state $a''(0)$ rotational distribution $N_{J''}$ is determined from measurements of the photofragment intensity for rovibrational bands that are not significantly perturbed by interactions with other singlet states. (Note that *all* states observed in the present work are perturbed to some degree by interactions with triplet continuum states that lead to predissociation; however, these are relatively weak perturbations that are not expected to significantly affect the excitation line strength.) Calculations of the electronic character of the upper states using the previously discussed diabatic state mixing model reveal that the $b'(v=12$ and $15)$ states are not significantly perturbed by other singlet states up to fairly high rotational levels; both of these states have almost pure b' character (greater than 93% b' up to $J=25$). These unperturbed states should exhibit regular absorption intensity distributions with constant electronic transition moments and vibrational overlaps, thus the rotational dependence of their absorption bands should be due exclusively to the Hönl–London rotational line strength factor. Provided that the predissociation fraction η remains constant for different rotational levels within these unperturbed states (a qualification which is justified by the results, as discussed in the following), it is possible to extract the rotational temperature of the $a''(0)$ molecules in the beam directly from the measured photofragment intensities using standard band analysis techniques.[40]

A laser scan of the unperturbed $b'(12)\leftarrow a''(0)$ band is shown in Fig. 3. The peak intensities of rotational transitions are found by fitting Gaussian functions to the photofragment signal peaks. The resulting fitted photofragment intensity as a function of lower state rotational level J'' and rotational energy is shown for the $b'(12)\leftarrow a''(0)$ R branch and the $b'(15)\leftarrow a''(0)$ P branch in Fig. 4; the other branch of each band yields similar results. Both bands exhibit the characteristic shape of excitation from a thermal rotational distribution as demonstrated by the straight line on the semilog

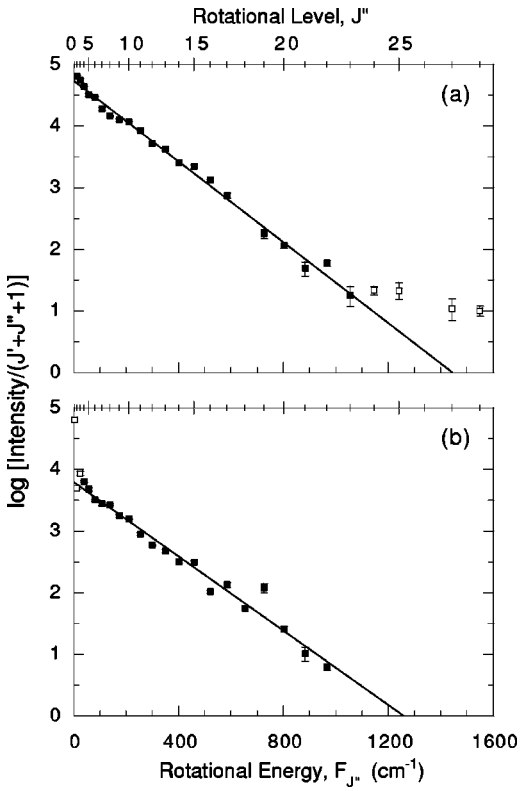

FIG. 4. Log[photofragment intensity/$(J'+J''+1)$] as a function of lower state rotational energy for (a) the $b'(12)\leftarrow a''(0)R$ branch; and (b) the $b'(15)\leftarrow a''(0)P$ branch. The measured values are shown by the squares; the error bars indicate counting statistics alone. The solid line gives the linear fit to the data over the range of lower state rotational levels from $J''=3-22$ (data points used in the fit are shown by the closed squares).

graph. (Note that in Fig. 4, the even/odd alternation of rotational level intensity due to nuclear spin statistics[40] has been artificially removed by multiplying the intensity of odd rotational levels by a factor of 2 in order to more clearly illustrate the nature of the rotational population.)

The effective rotational temperature of the $a''(0)$ molecules is obtained from the slope of the linear fit to $\log[N_{pJ'}/(J'+J''+1)]$ as a function of rotational energy for both the P and R branches of the $b'(12)$ and $b'(15)$ bands over the range $J''=3-22$.[40] The four bands yield similar rotational temperatures, with an average temperature of 433 ± 20 K. There was no significant difference in rotational temperature between the electron-impact and hollow-cathode ion sources. This is a reasonable temperature for the N_2^+ ions extracted from either ion source, as both sources operate above room temperature and there may be some additional rotational excitation in the ionization process. The close agreement between the measured photofragment intensities and the expected thermal distribution for the unperturbed $b'(12)$ and $b'(15)$ bands demonstrate the validity of the present technique for determining excitation line strengths.

While most of the intensity data are well-represented by the expected thermal behavior, Fig. 4 clearly shows that the measured values deviate from the straight line at both low and high J'': At low J'' the measured values scatter widely [most notably for $b'(15)$], while the measurements lie significantly above the expected line for $J''>23$ of $b'(12)$. The

deviations of the measured values from the expected behavior at the lowest and highest rotational levels occur for very different reasons. The measured photofragment intensities for the lowest rotational levels (upper state rotational level $J'<3$) are unreliable due to the possibility of rapid variation of the angular distribution for the dissociation process as a function of rotational level.[42] This variation in angular asymmetry leads to large changes in the collection efficiency of the detector for photofragments from the lowest rotational levels ($J'=0$, 1, and 2), and thus causes spurious photofragment intensity variations. At higher rotational levels, the asymmetry parameter for the dissociation quickly approaches an asymptotic value ($\beta \rightarrow 0.5$), and this asymptotic value is used to calculate the collection efficiency in the present analysis. Correction for changes in the fragment angular distribution are beyond the scope of the present work, hence only rotational levels $J' \geqslant 3$ are considered in the present analysis.

The origin of the deviation at high J'' ($J''>23$) is less clearly attributable, but several factors may be responsible. The lower state $a''(0)$ population may be nonthermal at high J'' due to rotational energy gained in the ionization process in the ion source or in collisions occurring either in the ion source or in the charge transfer reaction, thus leading to an enhancement of the population above $J''=23$. A second explanation of the enhanced population at high rotational levels may be that the lifetime of the metastable $a''(0)$ state is longer for high J'', thus leading to a greater survival probability for those molecules over the flight time from the charge transfer cell to the laser interaction region. Finally, the predissociation fraction for the upper state [e.g., $b'(12)$] may be larger for the higher rotational levels, leading to enhanced photofragment signals at high J'. The latter explanation appears to be unlikely, given that other rovibrational bands measured in the present work also yield higher than expected photofragment intensities for $J''>23$, which is consistent with an enhancement of the lower state population. Regardless of the origin of the deviation, it is apparent that the data may be unreliable at the highest rotational levels, therefore we restrict our present analysis to upper state rotational levels $J'<23$.

B. Photoexcited states

Determination of the rotational dependence of excitation and predissociation in the photoexcited states is facilitated by dividing the measured photofragment signal $N_{pJ'}$ in Eq. (6) by the lower state $a''(0)$ population $N_{J''}$, which is the Boltzmann exponential factor at the measured rotational temperature of 443 K. For unperturbed bands, the photofragment intensity depends on rotational level only through the Hönl–London factor; however, in perturbed states both the predissociation fraction and the transition moments can vary with rotational level as well. Separate identification of these two effects is achieved by comparison of the measured photofragment intensities (which depend on both the excitation line strength and the predissociation fraction) to the calculated excitation line strengths (which do not include the effects of predissociation). In order to clearly isolate and characterize perturbations in the intensity spectra, the normal rotational dependence expected for unperturbed bands is factored out prior to comparison; both the experimentally measured photofragment intensity and the calculated line strength are divided by the Hönl–London rotational factor for each transition.

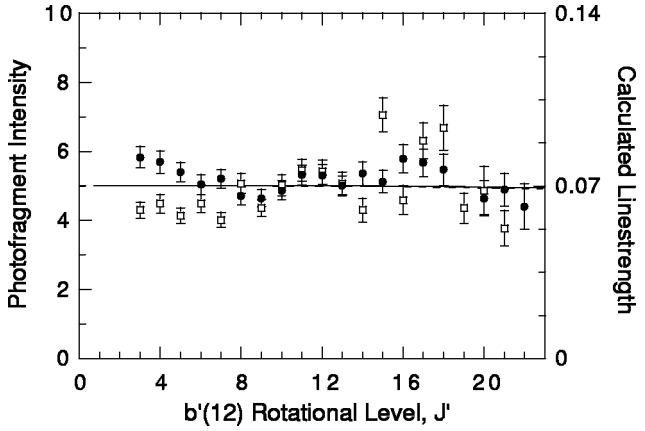

FIG. 5. $b'(12) \leftarrow a''(0)$ band measured photofragment intensity and calculated photoexcitation line strength as functions of upper state rotational level J': (●) R branch and (□) P branch measured photofragment intensities; (—) R branch and (- - -) P branch calculated line strengths. To reveal perturbations, both measured and calculated quantities have been divided by the (unperturbed) Hönl–London rotational line strength factor for the transition, and the photofragment intensity is further divided by the Boltzmann exponential factor for the rotational population of the $a''(0)$ lower state (see the text). The displayed photofragment intensity is relative to this band only and the magnitude should not be compared to that shown for other bands in Figs. 6–11; however, the magnitude of the calculated line strength can be compared directly to that shown for other bands.

The results for individual bands are discussed in the following, which begins with a demonstration of the analysis technique for the unperturbed $b'(12)$ and $b'(15)$ bands, and then proceeds to an analysis of the highly mixed Rydberg-valence complexes $c'(3)/c(3)/b'(10)$ and $c'(4)/c(4)/b'(13)$.

1. $b'(12)$ and $b'(15)$

The scaled photofragment intensity, divided by the Boltzmann exponential for the lower state population and the Hönl–London factor, as a function of upper state rotational level J' for the $b'(12) \leftarrow a''(0)$ band is shown in Fig. 5. Also shown on the graph is the calculated photoexcitation line strength from Eq. (5) divided by the same Hönl–London factors. As a note of caution, the magnitude of the displayed photofragment intensity is relative to each individual band alone, so that the displayed magnitude should not be compared to other bands. However, the displayed calculated line strength can be compared from one band to the next to provide an assessment of overall band strength.

The graph shows that both the scaled measured and calculated intensities are constant for the $b'(12)$ band, indicating that the intensity distribution is normal and that the state is indeed unperturbed; the $b'(15)$ band yields a similar graph. The present observation of a constant predissociation fraction throughout the $b'(12)$ state is confirmed by direct measurements of η for several individual rotational levels using the metastable molecule depletion technique developed

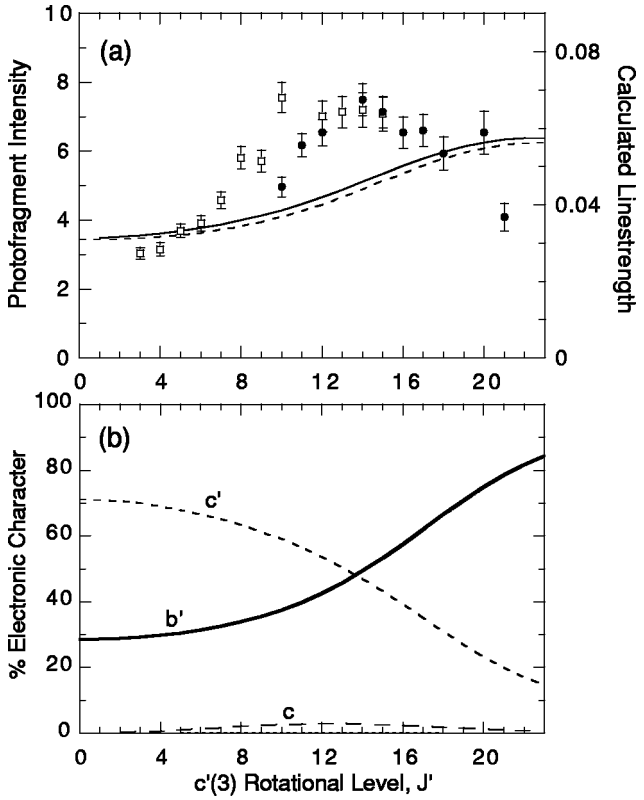

FIG. 6. (a) $c'(3)\leftarrow a''(0)$ band measured photofragment intensity and calculated photoexcitation line strength as functions of upper state rotational level J', as in Fig. 5. (b) Percentage diabatic electronic state character of the nominal $c'(3)$ rotational levels calculated from the state mixing model, as discussed in the text.

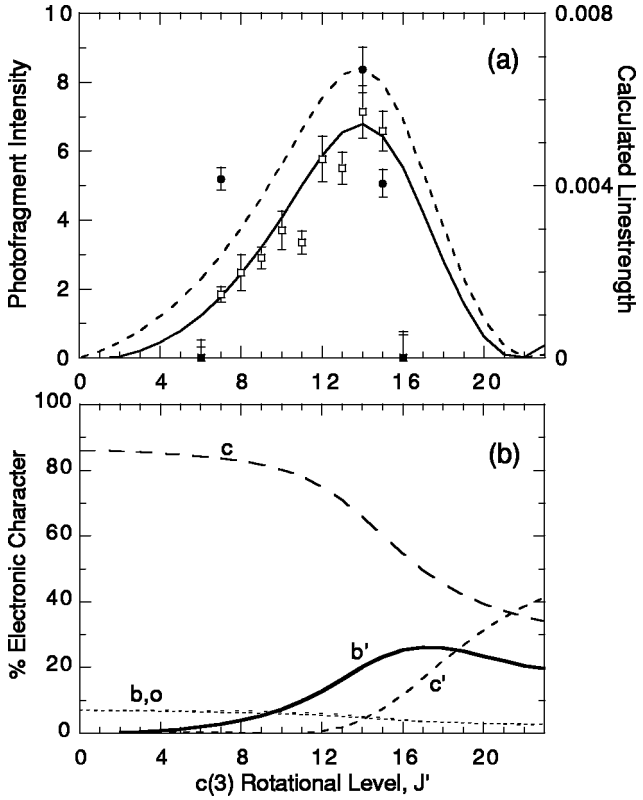

FIG. 7. (a) $c(3)\leftarrow a''(0)$ band, as in Fig. 5. (b) Calculated diabatic electronic state character of the nominal $c(3)$ state.

previously in our lab.[29] Several data points shown in the graph scatter significantly from the overall constant behavior due to random variations in laser-neutral beam overlap and fitting uncertainties due to the small number of frequency-stepped data points on each peak (3–5 steps). These variations limit the sensitivity to localized changes in the predissociation fraction η to the 10%–20% level using the present technique.

2. The $c'(3)/c(3)/b'(10)$ complex

The $c'(3)$ and $c(3)$ Rydberg states are highly mixed with each other and with the $b'(10)$ valence state. The strong rotational dependence of the mixing leads to significant shifts in the energy levels and causes rapid variations in intensity within the rovibrational bands. The scaled measured photofragment intensities and calculated transition line strengths for the $c'(3)$, $c(3)$, and $b'(10)$ bands are shown in Figs. 6, 7, and 8, respectively. Also shown in these figures is the calculated fractional diabatic electronic state character of each nominal state as a function of rotational level.

In the $c'(3)$ band, the measured photofragment intensity roughly doubles as the rotational level increases from 4 to 12 and then levels off with a slight decrease at higher J. The calculated excitation line strength shows a similar increase in intensity, however the increase begins at slightly higher J and is more gradual over the range from $J=6$ to 20 before leveling off. The increase in transition strength is due to the homogeneous interaction $c'(3)-b'(10)$ that mixes into the nominal $c'(3)$ state a substantial fraction of diabatic b' character, which increases from 30% at $J=4$ to over 80% at $J=23$. The present results for the fractional electronic character of $c'(3)$ are essentially identical to the calculations of Edwards *et al.*[33] The vibrational overlap between $a''(0)$ and the diabatic $b'(10)$ state is $\sim$25 times greater than for the diabatic $c'(3)$ state, thus the increase in b' character significantly enhances the transition strength for the high J levels of $c'(3)$. Enhanced absorption intensity at high rotational levels was also observed in the $c'(3)\leftarrow X(0)$ absorption band by Yoshino, Freeman, and Tanaka[16] and similarly ascribed to increased valence character acquired through homogeneous interaction with $b'(10)$.

Although the overall patterns of measured photofragment and calculated excitation intensities are similar in $c'(3)$, the photofragment intensity rises more sharply than the calculated line strength, reaches a maximum in the range $J=10-14$, and then decreases for $J>14$. The difference between photofragment and excitation intensities may be due to an increase in the predissociation fraction η over the range from low to medium rotational level, followed by a decrease in predissociation at higher J. Previous direct measurements of η for $c'(3)$ show that it increases moderately from 0.51 ± 0.05 at $J=9$ to 0.70 ± 0.15 at $J=13$.[29]

The predissociation trends observed for $c'(3)$ in the present work are in good qualitative agreement with two previous studies using different experimental techniques. The linewidths of $c'(3)\leftarrow a''(0)$ rotational transitions measured by Kam *et al.*[25] show a gradual increase over the range

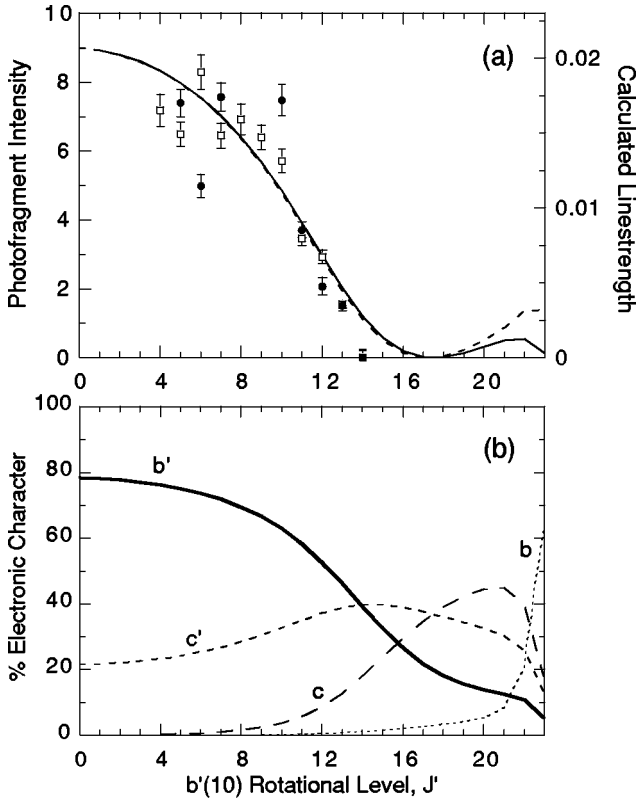

FIG. 8. (a) $b'(10) \leftarrow a''(0)$ band, as in Fig. 5. (b) Calculated diabatic electronic state character of the nominal $b'(0)$ state.

$J=3-12$ before leveling off at higher J, indicating stronger predissociation (shorter lifetimes) of the medium rotational levels. Ajello, James, and Ciocca[23] recently determined relative η values for individual rotational levels of $c'(3)$ and $c'(4)$ by comparison of measured emission intensities to calculated excitation intensities. Their results for $c'(3)$ show that the predissociation yields reach a maximum in the medium J range ($5<J<11$), and then decrease for higher J. The increased predissociation from low to medium J is due to the increased percentage of diabatic b' character of these levels, which is consistent with the previously suggested role of the b' state as an intermediary to predissociation via the triplet continuum.[25,27–29] However, there does not appear to be a ready explanation for the observed leveling off and slight decrease of predissociation at higher J, given that the percentage b' character continues to increase.

The dependence of photofragment intensity on b' character is also observed for the $c(3)$ band (see Fig. 7). While no photofragments are observed in $c(3)$ for rotational levels below $J=6$, the photofragment intensity increases rapidly from $J=7$ to a peak at $J=14$, before dropping back to zero at $J=16$ and above. This behavior is closely matched by the calculated line strength which is very weak at low J, rises to a peak at $J=14$, and then drops essentially to zero at high J. The strong transitions observed for the $c(3)$ band at medium J are due to intensity borrowing from $b'(10)$. The fractional b' character acquired through the heterogeneous interaction $c(3)-b'(10)$ rises from 1% at $J=5$ to a maximum of 25% at $J=16$; this substantial b' character provides enhanced vibrational overlap with the $a''(0)$ state. Although the b' character remains greater than 20% up to $J=23$, the calculated line strength drops rapidly to near zero at $J=21$ due to destructive interference between adjacent vibrational levels of the diabatic b' state ($v=9$, 10, 11, and 12) whose contributions to the transition moment tend to cancel. The drop in intensity is somewhat more rapid in the measured photofragment signal than in the calculation, possibly indicating that a decrease in predissociation fraction accompanies the loss of b' character.

There is also a significant difference in intensity between the R and P branches in the photofragment spectrum of the $c(3)$ band, with the R branch transitions to $J=7$ and 14 observed to be considerably stronger than their P branch counterparts. This anomalous R/P intensity is due to the mixed $\Pi-\Sigma$ character of the $c(3)$ state which leads to differences in interference in the transition moments for the R and P branches. The present case of transition from a pure $^1\Sigma$ state [the $a''(0)$ state] to a mixed state of $^1\Pi$ and $^1\Sigma$ character is discussed by Lefebvre-Brion and Field,[36] who show that the sign of the transition moment for the Π components is reversed for the R and P branches, while the sign of the Σ transition moments remains the same. This leads to constructive interference in one branch and destructive interference in the other, and thus an intensity difference between the R and P branches.

The largest contributions to the $c(3)$ transition moment from states of Π character actually come not from the diabatic $c(3)$ state itself, but rather from the diabatic $o(3)$ state and several lower vibrational levels of the diabatic b state. Although these states make up only a small fraction of the electronic character of the perturbed $c(3)$ state, they have much better vibrational overlaps with $a''(0)$ than does the diabatic $c(3)$ state, and therefore provide larger transition moments. Although the present calculations correctly predict the magnitude of the R/P intensity deviation, the calculations incorrectly show the P branch as stronger due to constructive interference. The R branch suffers destructive interference in the calculations, but it is the enhanced branch in the observed photofragment intensity. The source of this discrepancy must be a relative sign error between the Π and Σ transition moments, however it is difficult to isolate where the sign error originates, given the large number of diabatic states that contribute to the nominal $c(3)$ state and the fact that each transition moment is the product of three signed quantities (basis state coefficient, electronic transition moment, and vibrational overlap integral).

The photofragment intensity for the $b'(10)$ band is strong at low J, but smoothly drops with increasing rotational level to near zero at $J=14$ (see Fig. 8). The calculated line strength shows a nearly identical decrease. The calculated electronic character of $b'(10)$ reveals that the decrease in intensity is primarily due to the loss of diabatic b' character in the interactions with $c'(3)$ and $c(3)$. In addition, there is increasingly destructive interference among the transition moments associated with the diabatic $b'(10)$ level and other b' vibrational levels as the rotational level increases. The very good agreement between the photofragment intensity and the calculated excitation line strength indicates that

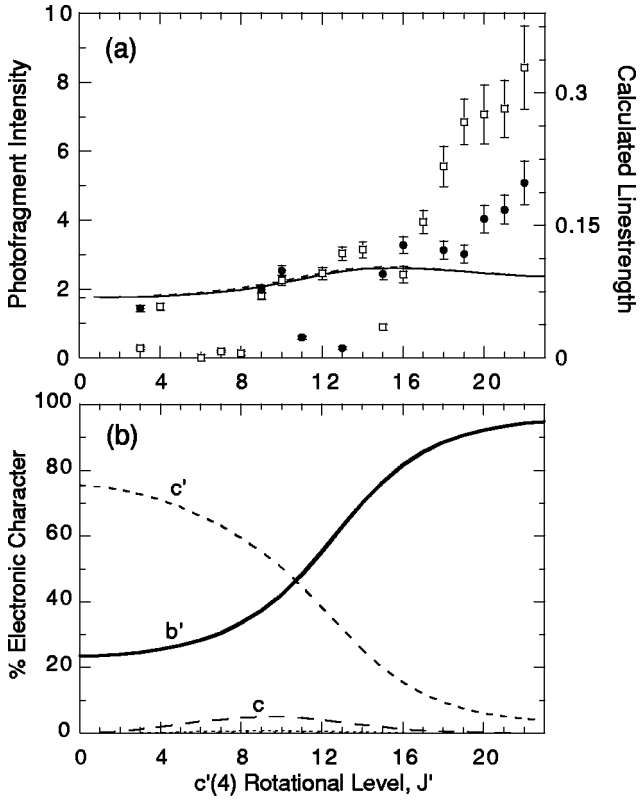

FIG. 9. (a) $c'(4)\leftarrow a''(0)$ band, as in Fig. 5. (b) Calculated diabatic electronic state character of the nominal $c'(4)$ state.

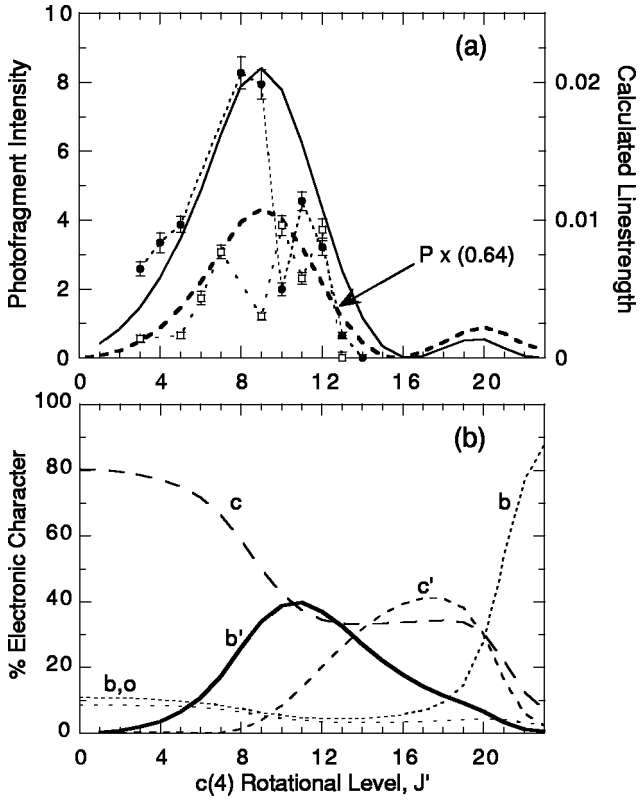

FIG. 10. (a) $c(4)\leftarrow a''(0)$ band, as in Fig. 5. (b) Calculated diabatic electronic state character of the nominal $c(4)$ state.

the predissociation fraction does not change significantly over the observed range of rotational levels up to $J=13$.

3. The $c'(4)/c(4)/b'(13)$ complex

A similar complex is formed by the next higher vibrational level of the Rydberg states, in which $c'(4)$ and $c(4)$ interact with $b'(13)$ in much the same manner as observed for the lower complex. A graph of the term energies of these states as a function of rotational level is shown in Fig. 2. Note that in the present work, we follow the $c(4)$ state adiabatically beyond its strong interaction with the $b'(13)$ state and label the middle energy state of this complex as $c(4)$ and the upper energy state as $b'(13)$ for all rotational levels. This is consistent with our previous assignment,[27–29] but differs from the labeling above the crossing adopted by Yoshino, Freeman, and Tanaka.[16] The assignment of Yoshino, Freeman, and Tanaka was based on a 2×2 deperturbation of the heterogeneous interaction $c(4)-b'(13)$ alone; this isolated deperturbation scheme called for an interchange of labels above $J=9$ for $b'(13)$ and $c(4)$ as the two states apparently cross. The larger scale deperturbation model used in the present work shows that there is actually a large range of rotational levels involved in this interaction and that there is substantial mixing of $b'(13)$ and $c(4)$ with other electronic states (e.g., c' and b) in this range. Given these considerations, we prefer to use the adiabatic labeling scheme which allows the changes in character to be clearly tracked.

The intensity patterns observed for the $c'(4)$, $c(4)$, and $b'(13)$ bands are similar to those observed in the $c'(3)/c(3)/b'(10)$ complex, and interpretation of the variations follows along much the same lines. The scaled photofragment intensity as a function of rotational level is graphed together with the calculated transition line strength for the $c'(4)$, $c(4)$, and $b'(13)$ bands in Figs. 9, 10, and 11, respectively. The calculated fractional diabatic electronic state characters are shown in part (b) of each figure.

The photofragment intensity of the $c'(4)$ band increases with rotational level, showing a gradual strengthening up to $J=17$, and then a much sharper increase in the range $J=18-22$. Also, a substantial difference in intensity of the P and R branches is observed for the high J levels, with the P transitions having almost double the intensity of the R transitions. The calculated excitation line strength also increases with rotational level; however, the increase is less pronounced and the calculated transition intensity remains constant for $J>16$. The variations in intensity clearly result from the enhanced b' character of the state as the rotational level increases; the b' character changes from 20% at low J to over 90% at high J. The observed moderate rotational dependence of predissociation is in agreement with the linewidth measurements for $c'(4)$ made by Helm, Hazell, and Bjerre,[27] which show that the absorption linewidths increase with J as the result of lifetime shortening due to stronger predissociation. The η factors for $c'(4)$ determined recently by Ajello, James, and Ciocca[23] from the emission spectra also show that predissociation increases with rotational level over the range of their experiment from $J=0$ to 13.

The measured photofragment intensity is significantly larger than the calculated excitation line strength at high J

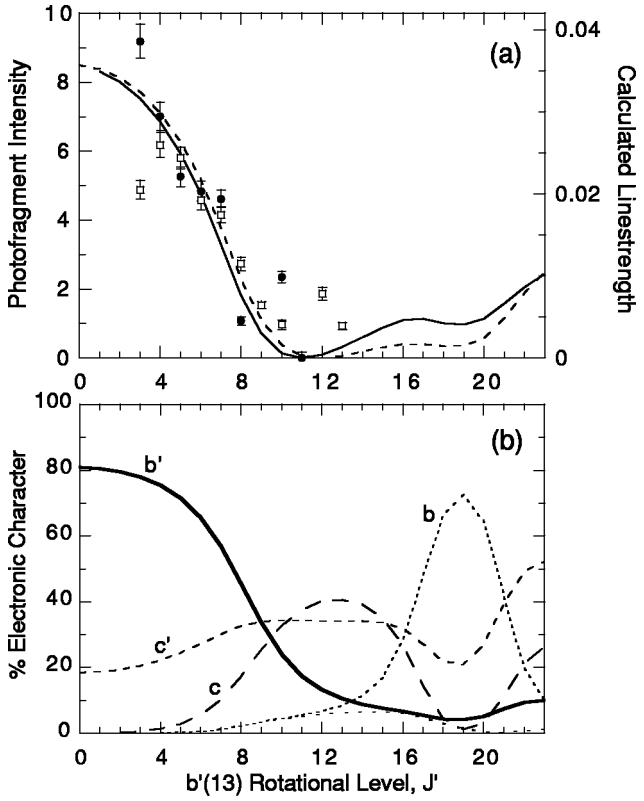

FIG. 11. (a) $b'(13)\leftarrow a''(0)$ band, as in Fig. 5. (b) Calculated diabatic electronic state character of the nominal $b'(13)$ state.

($J=18-22$) in the $c'(4)$ state. This difference may arise either from much stronger predissociation of these rotational levels or from calculated excitation strengths that are too small for the highest rotational levels. Given that the measured predissociation fraction at $J=9$ is 0.62 ± 0.08,[29] the predissociation fraction can increase by at most a factor of 1.6 above its value at $J=9$. However, if the predissociation rate increases, the increased transition linewidth would lead to an enhancement of the number of molecules photoexcited because of the broad linewidth of the laser, which is larger than the expected transition linewidths.[27] Thus, it appears that the observed increase in the photofragment intensity of greater than a factor of 3 from $J=9$ to $J=22$ (see Fig. 9) must be due in large part to increases in the photoexcitation strength, rather than solely due to increases in the predissociation fraction. It should also be noted that an enhancement of the absorption strength at high J was observed in the $c'(4)\leftarrow X(0)$ band by Yoshino, Freeman, and Tanaka,[16] however the increase in absorption strength could not be quantified in their experiments. A second observation that calls into question the accuracy of the calculated line strengths at high J is the observed difference in intensity of the P and R branches in $c'(4)$, which is not predicted by the model calculations.

While the fractional b' character of the $c'(4)$ state increases by a factor of 4 from low to high J, the calculated excitation line strength increases by less than a factor of 1.5 over this range. This is a very surprising result at first sight, given the much better vibrational overlap of the $a''(0)$ lower state with the $b'(13)$ diabatic state than with the $c'(4)$ diabatic state. The resolution of these seemingly disparate observations lies in interference between the various b' vibrational levels that contribute to the transition moment. At low J, several diabatic b' vibrational levels (primarily $v=12$, 13, and 14) contribute to the character of the $c'(4)$ state and the transition moments of the various levels add together with the same phase, leading to constructive interference in the line strength. This interesting effect was first noted by Stahel, Leoni, and Dressler[31] in their calculations of intensities for transitions to both $c'(4)$ and $c'(3)$ from the ground state. As the rotational level increases, the total b' character of the $c'(4)$ state increases, however at higher J the $b'(13)$ level alone dominates the electronic character with a basis state coefficient of greater than 0.95. The consolidation of b' character into a single vibrational level removes the constructive interference between adjacent vibrational levels that occurs at lower J. The result of the loss of interference enhancement is that the calculated line strength increases only rather weakly with total b' character in this case.

Several transitions in the $c'(4)$ band are unexpectedly weak in both the P and R branches, most notably those reaching $J=6$ and 8. The model calculations do not show these intensity perturbations, suggesting that these anomalies may be the result of localized perturbations in the interactions between the singlet and triplet states.[28]

The $c(4)$ band (shown in Fig. 10) is observed to have appreciable photofragment intensity only over the range from $J=3$ to 13. The photofragment intensity rises rapidly with increasing rotational level up to a maximum near $J=9$ and then drops sharply with no transitions observed above $J=13$. The calculated line strength correctly predicts the rotational level range of significant photofragment production, which clearly results from a large admixture of b' character (up to 40%) in this J range acquired through the heterogeneous interaction $c(4)-b'(13)$.

There is a substantial difference in the observed intensity between the R and P branches of the $c(4)$ band, which is even more pronounced than that observed in the $c(3)$ band. The origin of this anomaly is again the interference between the Π and Σ transition moments.[36] In this case, the calculations correctly predict that the R branch is stronger, however the difference between the R and P branches is larger in the measured photofragment intensities than in the calculated line strengths (note that in Fig. 10, the calculated line strength for the P branch has been multiplied by a factor of 0.64 to match the measured photofragment intensity). The largest contributions to the $c(4)$ transition moment from states of Π character come from the diabatic $o(4)$ state and several lower vibrational levels of the diabatic b state. The calculations appear to underestimate the contributions from these states, resulting in less variation between the R and P branch intensities than is actually observed.

The $b'(13)$ band shows strong photofragment intensity at low rotational levels, but rapidly decreases until it is lost above $J=13$. This behavior is closely matched by the calculated line strengths, which reveal that the decrease in intensity is primarily due to the loss of b' character in the interaction with $c'(4)$ and $c(4)$. In addition, destructive interference of the transition moments for the diabatic

$b'(13)$ and $b'(14)$ states at higher J causes the intensity to drop off more rapidly than the decrease in total b' character.

Although the strong Rydberg–valence interactions lead to rapid changes in excitation line strengths for the $c(4)$ and $b'(13)$ states, the present results do not indicate large changes in the predissociation fractions for the observed rotational levels of these states. The close agreement between the observed photofragment intensities and the calculated excitation line strengths shows that the predissociation fractions vary by less than 10%–30% for all of the observed upper levels. The consistently strong predissociation for the rotational levels of these states is not surprising, given that the observed levels all have substantial character of the diabatic b' state, which is the intermediary to the triplet states leading to predissociation in this energy range.[27–29]

4. Unobserved states

Several electronic states that lie in the present energy range are not observed in the photofragment spectra despite having symmetries that allow dipole transitions from the $a''(0)$ state. No transitions are observed to the nominal $b(v=13–19)$ states, although these states are expected to be completely predissociated.[21] This lack of observation is consistent with the fact that transitions to these states are calculated to be too weak for observation in the present experiments, largely because of the poor vibrational overlap of these b states with $a''(0)$, as can be seen from the potential energy curves in Fig. 1.

While the P and R branches are observed for excitation of the $c(3)$ and $c(4)$ $^1\Pi_u^+$ states, the Q branch transitions for excitation of the Π^- components of these states are very weak, if they appear at all, in the photofragment spectra. The enhancement of the P and R branches is due to intensity borrowing from the neighboring b' $^1\Sigma_u^+$ states through the heterogeneous interaction $b'(\Sigma^+)–c(\Pi^+)$. However, the Π^- levels are not affected by this interaction, and therefore the Q branch transitions are much weaker by comparison.

V. CONCLUSION

In the present study, we have measured the photofragment intensity distributions arising from photoexcitation of the $a''(0)$ state to eight vibrational states of singlet nitrogen. The photofragment spectra show strong departures from the normal, unperturbed rovibronic distributions due to extreme mixing of electronic state character in the interaction of the c' and c Rydberg and b' valence states. Calculations based on the diabatic state deperturbation model originally developed by Stahel, Leoni, and Dressler,[31] with the inclusion of rotational interactions,[27] are in excellent agreement with the intensity variations observed for most bands. The results confirm that b' electronic character is the dominant contributor to transition strength from $a''(0)$ in this energy range and demonstrate the importance of interference in the absorption intensity.

The calculations based on the theoretical model accurately predict most of the intensity variations in excitation of the highly mixed $c'(3)/c(3)/b'(10)$ and $c'(4)/c(4)/b'(13)$ complexes. The intensity for both the $b'(10)\leftarrow a''(0)$ and $b'(13)\leftarrow a''(0)$ bands drops rapidly with rotational level as the states lose their b' character due to homogeneous interaction with the c' state and in more localized heterogeneous interaction with the c state. In both bands, the decrease in intensity is hastened by destructive interference between adjacent vibrational levels of the b' diabatic state. The $c(3)\leftarrow a''(0)$ and $c(4)\leftarrow a''(0)$ bands acquire intensity in the medium rotational level range through the interactions $c(3)–b'(10)$ and $c(4)–b'(13)$, respectively.

Both the $c'(3)\leftarrow a''(0)$ and $c'(4)\leftarrow a''(0)$ bands increase in photofragment intensity with increasing rotational level from low to medium J; however, the $c'(3)$ band is observed to drop slightly at higher J, while the $c'(4)$ band continues increasing through the highest observed J. The enhancement in photofragment production from low to medium J can be partially explained by the increasing b' character of these states that leads to larger excitation line strengths. However, the observed photofragment intensity increases more rapidly than the calculated line strength, indicating that the predissociation branching fraction η increases moderately with rotational level for the $c'(3)$ and $c'(4)$ states. The diabatic b' state both facilitates photoexcitation and acts as an intermediary for predissociation of these states. This finding is in agreement with previous linewidth measurements for rotational transitions in $c'(3)$[25] and $c'(4)$[27] and with the recent determinations of predissociation branching fractions for individual rotational levels of these states by Ajello, James, and Ciocca.[23]

The present results confirm the validity of the diabatic state mixing model developed by Stahel, Leoni, and Dressler for states in this energy range and demonstrate its predictive power. The model can be used to calculate absorption strengths, and emission branching and oscillator strengths for the singlet states of nitrogen, including the atmospherically most important $c'(0)$ state. The dramatic intensity variations observed in the present work highlight the necessity to consider perturbations in detail for accurate modeling of absorption and emission spectra, energy transfer, and odd-nitrogen chemistry in planetary atmospheres where N_2 is an important component.

ACKNOWLEDGMENTS

We thank Dr. D. L. Huestis for helpful discussions during the course of this work. The experiments were performed at SRI International. This material is based upon work supported by the National Science Foundation under Grant No. ATM-9411600. C.W.W. acknowledges partial support by Denison University. H.H. acknowledges partial support by the Deutsche Forschungsgemeinschaft through SFB276TP13.

[1] P. G. Richards, D. G. Torr, and M. R. Torr, J. Geophys. Res. B **86**, 1495 (1981).
[2] D. F. Strobel, R. R. Meier, M. E. Summers, and D. J. Strickland, Geophys. Res. Lett. **18**, 689 (1991).
[3] M. H. Stevens, R. R. Meier, R. R. Conway, and D. F. Strobel, J. Geophys. Res. B **99**, 417 (1994).
[4] E. C. Zipf, P. J. Espy, and C. F. Boyle, J. Geophys. Res. B **85**, 687 (1980).
[5] S. Solomon, Planet. Space Sci. **31**, 135 (1983).

[6] V. I. Schematovich, D. V. Bisikalo, and J. C. Ge'rard, Ann. Geophys. (France) **10**, 792 (1992).
[7] R. D. Hudson and V. L. Carter, Can. J. Chem. **47**, 1840 (1969).
[8] E. C. Zipf and R. W. McLaughlin, Planet. Space Sci. **26**, 449 (1978).
[9] The $^3\Pi_u$ and $2\,^3\Sigma_u^+$ potential energy curves in Fig. 1 represent the *ab initio* calculations of Refs. 43 and 44, respectively, adjusted to the experimental separated atom limits. Potential energy curves for the singlet *ungerade* states are the unperturbed diabatic states of Ref. 31. The remaining curves in Fig. 1 are taken from Ref. 45 and extrapolated to the adiabatic dissociation limits defined by Ref. 44.
[10] A. Lofthus, Can. J. Phys. **35**, 216 (1957).
[11] S. G. Tilford and P. G. Wilkinson, J. Mol. Spectrosc. **12**, 231 (1964).
[12] P. K. Carroll and C. P. Collins, Can. J. Phys. **47**, 563 (1969); P. K. Carroll, C. P. Collins, and K. Yoshino, J. Phys. B **3**, L127 (1970); P. K. Carroll and K. Yoshino, *ibid*. **5**, 1614 (1972).
[13] K. Dressler, Can. J. Phys. **47**, 547 (1969).
[14] K. Yoshino, Y. Tanaka, P. K. Carroll, and P. Mitchell, J. Mol. Spectrosc. **51**, 87 (1975).
[15] K. Yoshino and Y. Tanaka, J. Mol. Spectrosc. **66**, 219 (1977).
[16] K. Yoshino, D. E. Freeman, and Y. Tanaka, J. Mol. Spectrosc. **76**, 153 (1979).
[17] J.-Y. Roncin, F. Launay, and K. Yoshino, Planet. Space Sci. **35**, 267 (1987).
[18] J.-Y. Roncin, F. Launay, J.-L. Subtil, and K. Yoshino, Planet. Space Sci. **39**, 1301 (1991).
[19] J.-Y. Roncin, J.-L. Subtil, and F. Launay, J. Mol. Spectrosc. **188**, 128 (1998).
[20] J. M. Ajello, G. K. James, B. O. Franklin, and D. E. Shemansky, Phys. Rev. A **40**, 3524 (1989).
[21] G. K. James, J. M. Ajello, B. O. Franklin, and D. E. Shemansky, J. Phys. B **23**, 2055 (1990).
[22] D. E. Shemansky, I. Kanik, and J. M. Ajello, Astrophys. J. **452**, 480 (1995).
[23] J. M. Ajello, G. K. James, and M. Ciocca, J. Phys. B **31**, 2437 (1998).
[24] H. Helm and P. C. Cosby, J. Chem. Phys. **90**, 4208 (1989).
[25] A. W. Kam, J. R. Lawall, M. D. Lindsay, F. M. Pipkin, R. C. Short, and P. Zhao, Phys. Rev. A **40**, 1279 (1989).
[26] W. Ubachs, L. Tashiro, and R. N. Zare, Chem. Phys. **130**, 1 (1989).
[27] H. Helm, I. Hazell, and N. Bjerre, Phys. Rev. A **48**, 2762 (1993).
[28] C. W. Walter, P. C. Cosby, and H. Helm, J. Chem. Phys. **99**, 3553 (1993).
[29] C. W. Walter, P. C. Cosby, and H. Helm, Phys. Rev. A **50**, 2930 (1994).
[30] W. Ubachs, Chem. Phys. Lett. **268**, 201 (1997).
[31] D. Stahel, M. Leoni, and K. Dressler, J. Chem. Phys. **79**, 2541 (1983).
[32] P. K. Carroll and Kh. I. Hagim, Phys. Scr. **37**, 682 (1988).
[33] S. A. Edwards, W.-Ü. L. Tchang-Brillet, J.-Y. Roncin, F. Launay, and F. Rostas, Planet. Space Sci. **43**, 67 (1995).
[34] C. W. Walter, P. C. Cosby, and H. Helm (unpublished).
[35] H. Helm and P. C. Cosby, J. Chem. Phys. **86**, 6813 (1987).
[36] H. Lefebvre-Brion and R. W. Field, *Perturbations in the Spectra of Diatomic Molecules* (Academic, Orlando, 1986), Chap. 5.
[37] The a'' potential curve is defined by the Rydberg–Klein–Rees (RKR) turning points derived from the constants: $\omega_e = 2188.33\ \mathrm{cm}^{-1}$, $\omega_e x_e = 21.245\ \mathrm{cm}^{-1}$, $B_e = 1.928\,25\ \mathrm{cm}^{-1}$, $\alpha_e = 0.0248\ \mathrm{cm}^{-1}$, $\gamma_e = -0.0071\ \mathrm{cm}^{-1}$, $Y_{00} = 0.369\ \mathrm{cm}^{-1}$, $T_0 = 98\,840.61\ \mathrm{cm}^{-1}$ relative to $X\ ^1\Sigma_g^+$ $(v=0,\ N=0)$.
[38] T. F. Hanisco and A. C. Kummel, J. Phys. Chem. **95**, 8565 (1991).
[39] A. W. Kam and F. M. Pipkin, Phys. Rev. A **43**, 3279 (1991).
[40] G. Herzberg, *Spectra of Diatomic Molecules* (Van Nostrand Reinhold, New York, 1950), Chaps. 3 and 4.
[41] W. J. van der Zande, W. Koot, J. Los, and J. R. Peterson, J. Chem. Phys. **89**, 6758 (1988).
[42] B. Buijsse, E. R. Wouters, and W. J. van der Zande, Phys. Rev. Lett. **77**, 243 (1996).
[43] S. L. Guberman, Geophys. Res. Lett. **18**, 1051 (1991).
[44] H. H. Michels, ''Electronic structure of excited states of selected atmospheric systems,'' in *The Excited State in Chemical Physics*, edited by J. W. McGowan (Wiley, New York, 1980).
[45] A. Lofthus and P. H. Krupenie, J. Phys. Chem. Ref. Data **6**, 113 (1977).